ELSEVIER

International Journal of Solids and Structures 41 (2004) 5837–5849

INTERNATIONAL JOURNAL OF SOLIDS and STRUCTURES

www.elsevier.com/locate/ijsolstr

Statistical homogenization for assemblies of elliptical grains: effect of the aspect ratio and particle orientation

Fabrice Emeriault *, Cécile Claquin

URGC Géotechnique, INSA Lyon, 34 avenue des arts, 69621 Villeurbanne, Cedex, France

Received 26 April 2004

Abstract

A statistical homogenization approach is used to determine the global behavior of granular assemblies of elliptical particles with a wide range of eccentricities. A first step is to define the statistical variables to use in the description of the granular arrangement and the evolution of their distribution with the particle aspect ratio and the sample creation procedure. This part is analysed through numerical simulations using the DEM code PFC^{2D}. Biaxial compression tests also provide the elastic characteristics of the different assemblies. Then the two proposed homogenization schemes can be applied (taking into account the conclusions of the numerical simulations) and their results compared with the DEM results. They proved to be strongly dependant on the distributions of the statistical variables and their correlation (for anisotropic initial arrangements particularly).

Keywords: Granular materials; Elliptical particle; Discrete element method; Anisotropy; Elasticity

1. Introduction

Homogenization approaches have been used in many recent studies to describe the global behavior of granular medium based on the knowledge of the microscopic characteristics of the material such as the interparticle contact law, the particle size distribution and initial arrangement (see for example the Proceedings of Powders and Grains, 1997 and 2001). Some of these developments called "statistical homogenization" consider that the fundamental parameter is the orientation of the normal to the contact plane between two particles and its statistical distribution.

Several hypotheses on the local–global relationships lead to upper and lower bounds for the global mechanical characteristics (generally referred as the kinematic and static scheme or approach). Different types of contact laws have been successfully introduced in the general concept of statistical homogenization and compared with experimental or numerical results: linear elasticity (Cambou et al., 1995; Chang and

* Corresponding author. Tel.: +33-472437926; fax: +33-472438520.
E-mail address: fabrice.emeriault@insa-lyon.fr (F. Emeriault).

0020-7683/$ - see front matter © 2004 Elsevier Ltd. All rights reserved.
doi:10.1016/j.ijsolstr.2004.05.047

Liao, 1994), Hertz-Mindlin nonlinear elasticity (Emeriault and Cambou, 1996), linear viscoelasticity (Emeriault and Claquin, 2000) or friction laws (Emeriault et al., 1996).

Nevertheless, all these developments consider the granular medium as an assembly of round particles (either disks or spheres) with narrow or wide range of radii. In order to enhance the theoretical description of the behavior of real or natural materials, more realistic particle shape should be considered. Dong and Pan (1999) and Emeriault (1997) have presented the first developments of a theoretical derivation of the global mechanical characteristics of granular materials assuming an elliptical shape of the particles. The proposed analyses fail to compare with experimental (Aloufi and Santamarina, 1995) or numerical results (Rothenburg and Bathurst, 1991, 1992) because the statistical description of the contact fabric is strongly influenced by the particle aspect ratio and the sample creation procedure (and the corresponding initial fabric).

Numerical simulations using the discrete element method with elliptical 2D particles or ellipsoids (3D) can be used to determine the evolution of both the distributions of the contact orientation, branch vector length and other interparticle contact features and the global characteristics such as elastic moduli and friction angles (Ng, 1994, 1999, 2001; Rothenburg and Bathurst, 1991, 1992; Ting et al., 1993, 1995; Claquin, 2003; Emeriault and Claquin, 2003).

The theoretical developments presented in this paper are based on simulations of the granular fabric and elastic behavior of assemblies of elliptical particles with the DEM code PFC^{2D} (Itasca Consulting Group, 1999). For the sake of simplicity, the results are restricted to the case of a linear elastic interparticle contact law.

2. Numerical simulations

The theoretical developments presented in Sections 3 and 4 are based on the analysis of numerical simulations performed with the discrete element method based code PFC^{2D}. These simulations correspond to biaxial compression tests of assemblies of 2000 elliptical grains with different aspect ratios and initial fabric. The considered granular media are assumed to contain identical elliptical particles characterized by their semi-major axis aR and semi-minor axis $bR = R/a$ (Fig. 1). Thus the area of each particle πR^2 is constant with the aspect ratio a^2. R is the *equivalent* radius of the particles. Furthermore, in order to avoid the formation of regular arrangements within the sample, it is necessary to define a grain size distribution. The following distribution has been used by several researchers because it captures accurately the behavior of a monosize medium (see for example Mahboubi, 1995):

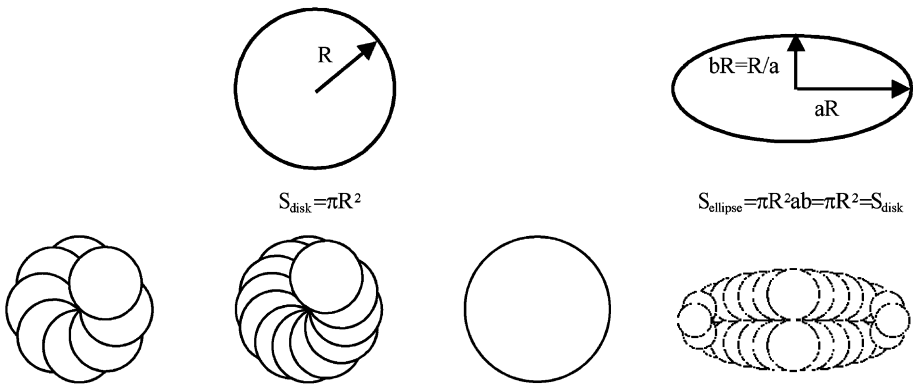

Fig. 1. Elliptical particles (theoretical and numerical representations).

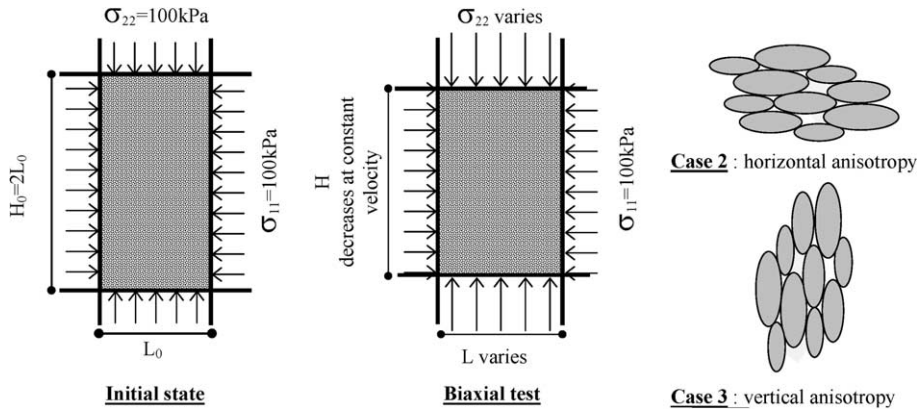

Fig. 2. Initial state and biaxial test.

- 40% of the particles have an equivalent radius of $0.8R$;
- 32.5% of the particles have an equivalent radius of R;
- 27.5% of the particles have an equivalent radius of $1.2R$.

The particle aspect ratio a^2 ranges from 1.0 to 3.0 and three cases of initial arrangement of particles are considered (see (Fig. 2)):

- Case 1: the particles are initially created with an isotropic distribution of the major axis orientation,
- Case 2: the particles are created with their major axis parallel to the horizontal direction,
- Case 3: the particles are created with their major axis parallel to the vertical direction.

The interparticle contact law is linear elastic (normal stiffness $k_N = 1.5\times10^7$ Nm^{-1}, tangential stiffness $k_T = k_N/1.5 = 1.0\times10^7$ Nm^{-1}) with a friction coefficient $\mu_p = 0.45$.

Even though PFC^{2D} only considers disks as basic granular elements, it is possible to define rigid assemblies of disks and thus represent elliptical grains (denoted as *clumps*) as illustrated in Fig. 1. The number of disks used depends on the particle aspect ratio and ranges from 12 for the reference circular case ($a^2 = 1.0$) to 32 for $a^2 = 3.0$.

The particles are compacted under isotropic stress (100 kPa), the effect of gravity is not considered and the interparticle friction coefficient is equal to 0.0 during compaction leading to rather dense samples.

In order to reduce the calculation time for the compaction step, the following procedure has been used:

- 2000 round particles of radius aR are created within a rectangular box (2:1 aspect ratio) with contact parameters $k_N = 1.5\times10^7$ Nm^{-1}, $k_T = 1.0\times 10^7$ Nm^{-1} and $\mu_p = 0.0$;
- the assembly is compacted by an inward movement of the horizontal and vertical walls of the box until an isotropic stress of 100 kPa is reached;
- the circular particles are replaced by the elliptical assemblies of disks with a random or fixed orientation of the major axis depending on the desired initial arrangement (Case 1, 2 or 3). The elliptical assemblies of disks present a global semi-major axis aR and a semi-minor axis R/a so that they perfectly fit (without any initial major overlap) in the void created by the deleted circular particles of radius aR;
- the confinement procedure is resumed until the particle velocities are smaller than 10^{-9} m s^{-1}.

During this last phase, the particle rotations are not restrained. Therefore the final orientation of the particle can slightly differ from the horizontal (resp. vertical) direction in Case 2 (resp. Case 3).

During all the calculation phases, the disk–disk contact stiffness is monitored in order to achieve a constant contact stiffness between elliptical grains whatever the number of disks of each particle involved in a contact. After a given number of calculation steps, the number n_c^i of disk–disk contacts involved in a contact i between two elliptical grains is determined. The corresponding normal interpenetrations u_N^i are calculated and the individual normal contact stiffness are modified according to the following rule:

$$k_N^{\text{disk}} = \frac{u_N^{\max}}{\sum u_N^i} k_N^{\text{elliptical grain}} \tag{1}$$

The tangential contact stiffness is also modified in order to verify $k_N^{\text{disk}} = 1.5 k_T^{\text{disk}}$. The updating procedure is validated by the simple following test. Two circular particles modeled by aggregates of 12 disks are brought into normal contact and the normal interpenetration is gradually increased (Fig. 3). If the disk–disk contact stiffness is not modified the normal contact force presents drastic variations with the total number of disk–disk contacts involved in the contact of the two aggregates. If the monitoring procedure is implemented, depending on the frequency of contact stiffness updating, a constant normal stiffness can be accurately modeled. In all the performed numerical simulations, contact stiffness is updated every 500 calculation cycles.

In addition to the contact stiffness update, one has to make sure that the considered modelling of elliptical grains does not introduce a surface roughness that will alter the results of the numerical simulations. Fig. 4 presents the results obtained with three different representations of circular grains (illustrated

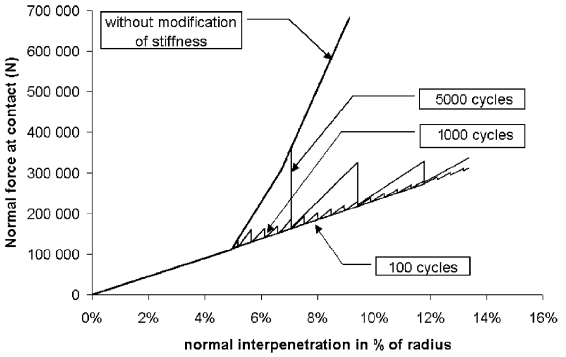

Fig. 3. Validation of the constant contact stiffness procedure.

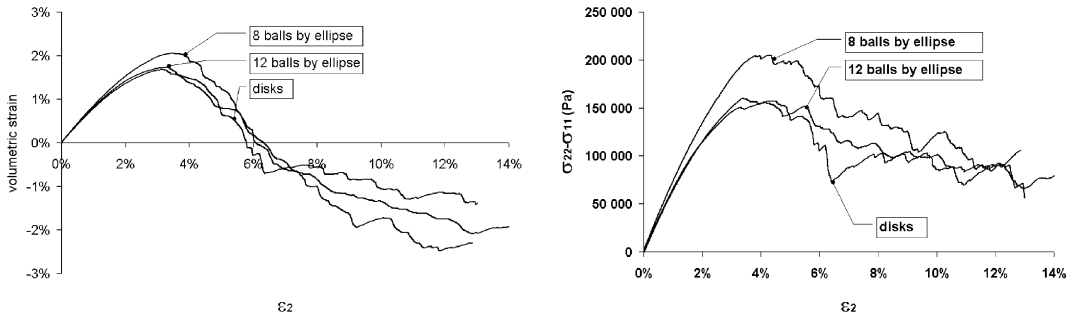

Fig. 4. Influence of the number of balls constituting the ellipsoidal particles.

Table 1
Number of disks used to model an elliptical grain with aspects ratio a^2

a^2	1.0	1.21	1.56	2.25	3.0
N	12	16	20	28	32

in Fig. 1); the reference case is that of single disks of radius R, the two others consider aggregates of either 8 or 12 small disks.

It appears that with 8 disks, the resulting circular grain present an additional friction induced by a geometrical surface roughness. This surface roughness is responsible for an increase in the global friction angle of approximately 15%. If the number of disks is increased to 12 per aggregate, this additional friction vanishes and the global behavior is identical to that of single disks of radius R. Therefore, for each shape factor analysed in the sequel, the number of disks N to use in an elliptical grain has been determined in order to minimize both the effect on the global behavior (decreasing with N) and the calculation time (increasing with N). The resulting values are reported in Table 1.

In Section 3, the statistical distributions of microscopic contact parameters such as contact orientations and branch vector length are determined from the initial states of each assembly and analytical approaches of these distributions are proposed for further use in theoretical developments (Section 5). In Section 4, the initial shear behavior (e.g. Young's modulus) of the different assemblies is analysed with respect to the particle shape factor and the initial isotropic or anisotropic arrangement of the grains. In Section 5, these results are compared with that of the statistical homogenization approach.

3. Contact between two elliptical particles

Unlike round particles, the contact between two elliptical particles a and b generally presents noncollinear contact plane normal vector and contact vector (joining the particle center to the contact point C). The length of the branch vector $\mathbf{l}^c$ (joining the centers of particles a and b) also depends on the position of the contact point C relatively to the centers of the two contacting particles (Fig. 5).

This implies that, in addition to the contact plane orientation θ (between 0 and 2π with the horizontal direction), the orientation of each particle major axis relatively to the contact plane should be considered as contact variables:

- θ_a denotes the orientation of particle a to the contact plane (between $-\pi/2$ and $+\pi/2$). Combined with θ and the particle shape factor a, this angle defines a contact vector $\mathbf{l}^{ac}$;
- similarly θ_b denotes the orientation of particle b to the contact plane (between $-\pi/2$ and $+\pi/2$) and defines with θ and a the contact vector $\mathbf{l}^{bc}$.

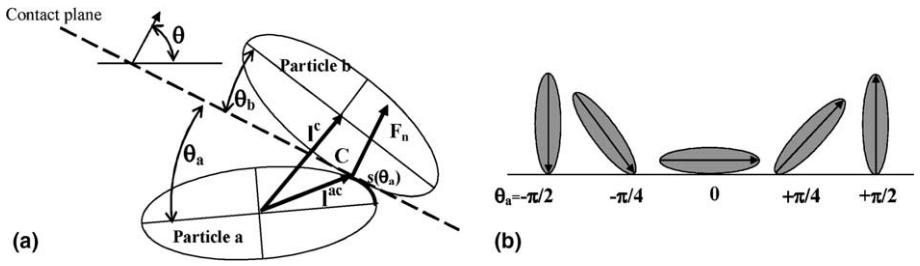

Fig. 5. (a) Contact between particles a and b and (b) orientation of particle to the contact plane.

The distribution of contacts within a representative element of volume can be described by θ, θ_a and θ_b considered as three statistical variables and their probability $P(\theta, \theta_a, \theta_b)$. If the three statistical variables are independent then $P(\theta, \theta_a, \theta_b) = P(\theta)P(\theta_a)P(\theta_b)$. Furthermore for isotropic distributions of the three variables $P(\theta, \theta_a, \theta_b) = 1/2\pi^3$.

The homogenization approaches presented in Section 5 are based on the knowledge of the distribution $P(\theta, \theta_a, \theta_b)$. The main difficulty lies in the determination of this probability and in particular its evolution with the particle aspect ratio a^2 and the assembly initial fabric. The careful analysis of the DEM simulations presented in Section 1 leads to major conclusions.

For all the samples created with an isotropic distribution of the particle orientation (Case 1), it appears that the three statistical variables are independent. Furthermore, $P(\theta)$ is isotropic and thus equal to $1/2\pi$. The distributions of angles θ_a and θ_b are independent but have the same expressions. The main conclusion that can be drawn from (Fig. 6 is that $P(\theta_a)$ and $P(\theta_b)$ are not isotropic and strongly depend on the particle shape factor a^2. The peaks in distribution occurring for angles of approximately $\pm 70°$ are essentially due to the modelling of the elliptical particles. These artefacts disappear when the shape factor increases.

The distributions of the orientation of the particles to their contact plane can be approached by the probabilities:

$$P(\theta_a) = \frac{\frac{ds}{d\theta_a}(\theta_a)}{s(\pi/2) - s(-\pi/2)} \quad \text{and} \quad P(\theta_b) = \frac{\frac{ds}{d\theta_b}(\theta_b)}{s(\pi/2) - s(-\pi/2)} \tag{2}$$

where $s(\theta_a)$ (resp. $s(\theta_b)$) is the arc length measured between the particle a (resp. b) major axis and the contact point C (Fig. 5).

Fig. 7 shows that the proposed approach gives a better description of the numerical results than the assumption of isotropy for both the distributions of particle orientation θ_a and θ_b and corresponding branch vector length. It is noteworthy that the assumption of isotropy leads to totally unacceptable results for the branch vector length distribution (see Fig. 7b). Nevertheless, differences can be observed in the distributions of θ_a, θ_b and $\mathbf{l}^c$. They can be explained to a certain extent by the grain size distribution considered in DEM simulations and that the theoretical approach does not account for. As mentioned by Ng (1999), the branch vector length distribution is constant with the shape factor a^2 provided that this distribution is normalized between the minimum and maximum possible values for $\mathbf{l}^c$.

In Cases 2 and 3, the three statistical variables are strongly correlated. The granular assemblies present a clearly anisotropic distribution of the particles orientation that does not depend on the aspect ratio (Fig. 8a) while the contact orientation distribution strongly depends on a^2 and can be accurately described by the empirical relationship Eq. (3):

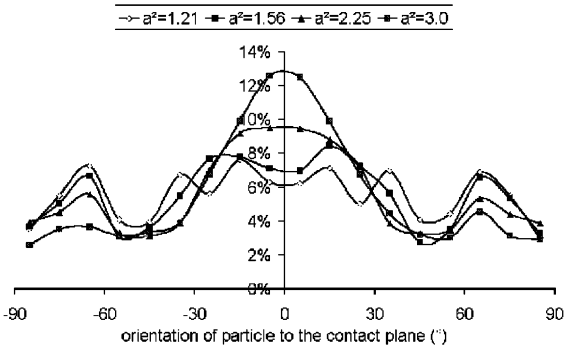

Fig. 6. Effect of the shape factor a^2 on the distribution of orientation of particle to the contact plane (Case 1).

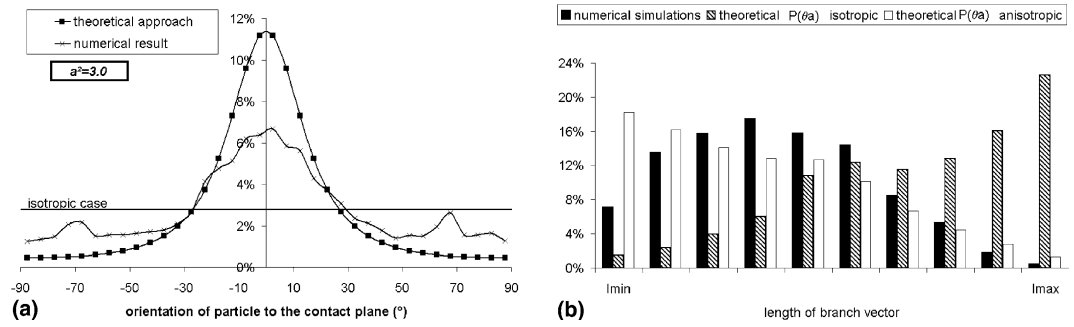

Fig. 7. (a) Probability of the particle orientation to the contact plane and (b) distribution of the branch vector length: numerical and theoretical results.

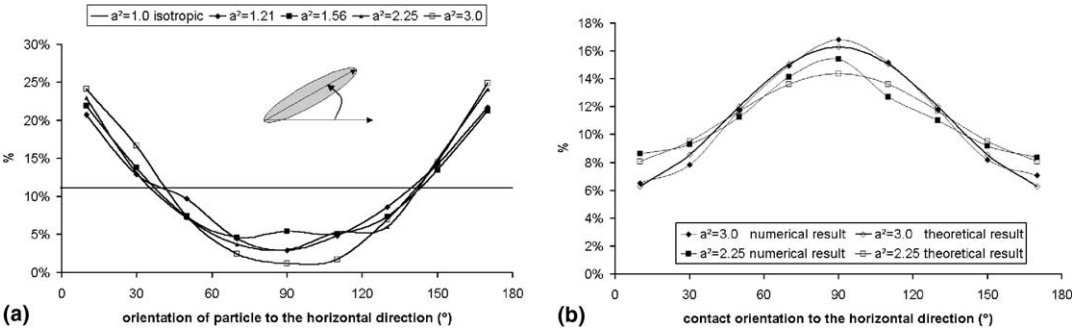

Fig. 8. (a) Distribution of the particle major axis orientation for Case 2 for different values of a^2 and (b) distribution of $P(\theta)$ for $a^2 = 2.25$ and 3.0 in Case 2.

$$P(\theta) = \frac{1}{2\pi}(1 - \phi\cos(2\theta)) \quad \text{with } \phi = \frac{1}{4}(a^2 - 1) \tag{3}$$

Fig. 8b gives an example of the accuracy of this analytical description of the contact orientation distribution. It has to be noted that even though the overall distribution of angles θ_a and θ_b is not affected by the anisotropy of the initial fabric (Fig. 9a), the orientation of the particles to the contact plane are strongly correlated to the contact orientation θ (Fig. 9b). Furthermore θ_a and θ_b appear to be not correlated:

$$P(\theta, \theta_a, \theta_b) = P(\theta)P(\theta, \theta_a)P(\theta, \theta_b) \tag{4}$$

A first approach of the distribution of θ_a and θ_b in the anisotropic Cases 2 and 3 assumes that the shape of the distribution is the same as in the isotropic case but with an offset θ_a^{max} depending on the contact orientation θ:

$$P_{aniso}(\theta, \theta_a) = P(\theta_a - \theta_a^{max}) \quad \text{where } \theta_a^{max} = \frac{\pi}{2} - \theta \tag{5}$$

$$P_{aniso}(\theta, \theta_b) = P(\theta_b - \theta_b^{max}) \quad \text{where } \theta_b^{max} = \frac{\pi}{2} - \theta \tag{6}$$

Both the effect of the shape factor a^2 and the anisotropy of the initial fabric can be accounted for by Eqs. (5) and (6).

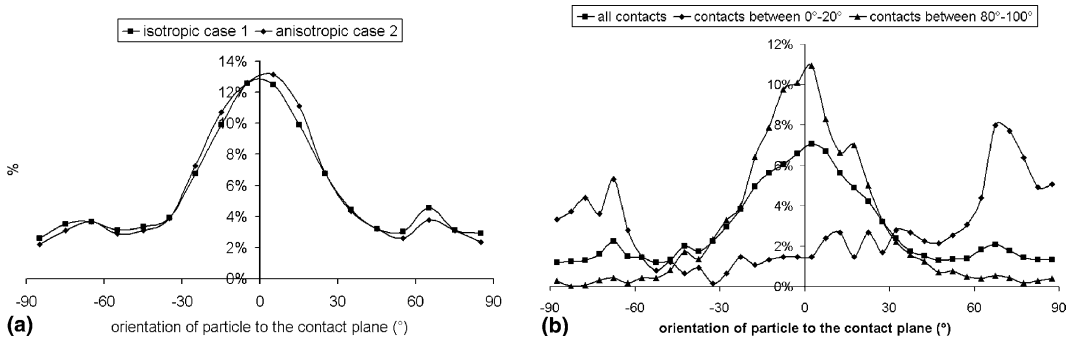

Fig. 9. (a) Overall distribution $P(\theta_a)$ for $a = 3.0$ in Cases 1 and 2, and (b) effect of the orientation of contact on the distribution of $P(\theta_a)$ for $a^2 = 3.0$ in Case 2.

4. Initial properties

For each considered shape factor ($a^2 = 1.21$, 1.56, 2.25 and 3.0), three cases of initial arrangement of the particles are considered. Case 1 corresponds to an isotropic distribution of the particle orientation within the assembly whereas Cases 2 and 3 correspond to anisotropic distributions (essentially horizontal for Case 2 and vertical for Case 3). This leads to 12 assemblies that have been analysed from a microscopic point of view in Section 3 and whose global characteristics and behavior are considered in the present section. The reference case is that of disks e.g. $a^2 = 1.0$. The analysis focuses on the initial porosity and linear elastic behavior of the assemblies but the biaxial compression tests have been performed up to a maximum of 12% in axial strain (beyond peak shear strength). Fig. 10 presents the results obtained in Case 1 for the different considered shape factor a^2. The analysis of the variation of shear strength with a^2 and the initial anisotropy of the fabric is beyond the scope of this paper.

Fig. 11 shows the measured initial porosity of the assemblies. As observed by Rothenburg and Bathurst (1991), the porosity of assemblies of elliptical particles depends on the shape factor. For values of a^2 close to 1.0, the porosity decreases by as much as 30%. Further increase in a^2 leads to looser assemblies. In the isotropic case, a maximum porosity seems to be reached for a^2 greater than 3.0 while the anisotropic assemblies present a growing porosity almost equivalent to that of the reference case of disks. It also appears that Cases 2 and 3 are very close, indicating that, even though the initial assembly presents a 2:1 aspect ratio, this does not affect the global characteristics.

The initial elastic moduli have been measured by applying to the assembly a 1% axial strain loading in one direction (either vertical or horizontal) while the stress is kept constant in the other direction. Therefore

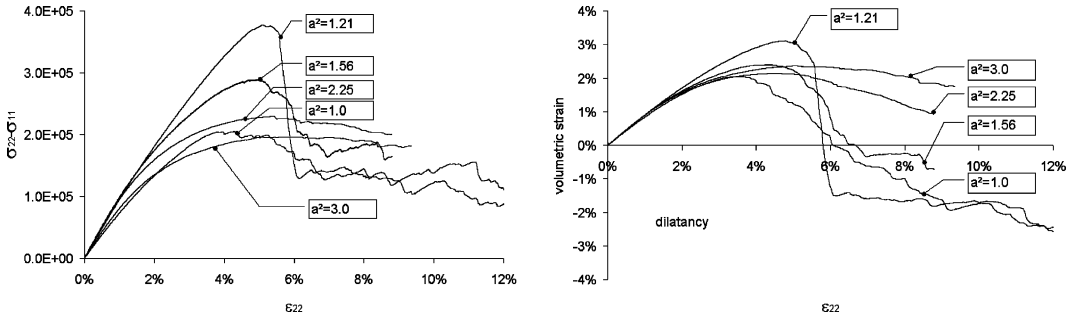

Fig. 10. Evolution of the deviatoric stress and volumetric strain during biaxial test.

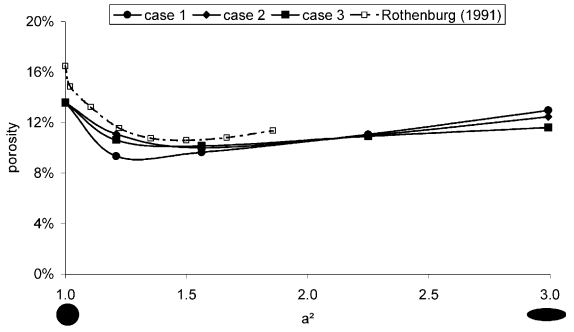

Fig. 11. Effect of the arrangement and shape factor on the porosity.

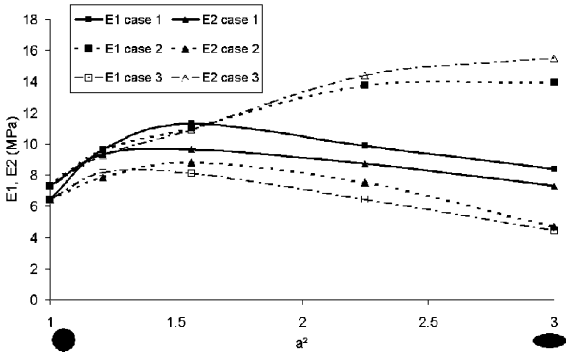

Fig. 12. Evolution of E_1 and E_2 with the shape factor and arrangement.

each sample is characterized by E_1 and E_2, elastic modulus in the horizontal and vertical direction. Fig. 12 presents the results obtained for Cases 1–3 and the different shape factors.

When the elliptical grains are initially created with a random orientation (Case 1), the resulting assembly is isotropic: the maximum deviation between E_1 or E_2 and their mean value is 7.3%. The variation of Young's modulus with the shape factor can be compared with that of the porosity. When a^2 increases from 1.0 to 1.56, the assembly becomes denser and thus stiffer. For greater values of a^2, the sample is looser and Young's modulus decreases.

Theoretically, the elastic moduli measured in Cases 2 and 3 should satisfy the following equation:

$$E_1(\text{Case 2}) = E_2(\text{Case 3}) \quad \text{and} \quad E_2(\text{Case 2}) = E_1(\text{Case 3}) \tag{7}$$

Fig. 12 shows that Eq. (7) is slightly not satisfied essentially because of the 2:1 aspect ratio of the initial sample. Nevertheless the difference never exceeds 5% of the mean value of the moduli. The anisotropic elastic behavior exhibited by the assemblies is increasing with the particle shape factor. For $a^2 = 3.0$, the deviation between E_1 or E_2 and their mean value is 52% and the ratio E_1/E_2 is greater than 3. In addition, if the elastic modulus in the direction parallel to the main particle orientation constantly increases with a^2, in the orthogonal direction the modulus first increases with a^2 up to 1.56 and then decreases.

5. Statistical homogenization approach

The statistical homogenization approach of the behavior of granular materials (proposed by Cambou et al., 1995; Chang and Liao, 1994) is based on two concepts: on one hand, within the Representative Element of Volume, stress and strain tensors are constant and localization or shear band formation is not considered; on the other hand, the number of particles within the RVE is sufficiently high so that all the interparticle contact parameters such as contact branch vector $\mathbf{l}^c$, contact force $\mathbf{F}$ and interpenetration $\mathbf{u}$ can be represented by their average value for defined statistical variables.

In previous developments assuming that the granular material is an assembly of round particles of radius R (without grain size distribution), it is straightforward to choose the contact plane normal vector $\mathbf{n}$ (or its orientation to the horizontal plane θ in 2D analysis) as the main statistical variable. The approaches proposed by Cambou et al. (1995) or Chang and Liao (1994) therefore consider the average values $\mathbf{l}(\mathbf{n}) = 2R\mathbf{n}$, $\mathbf{F}(\mathbf{n})$ and $\mathbf{u}(\mathbf{n})$ of the interparticle contact parameters presenting a normal contact vector of orientation $\mathbf{n}$. The main element of these approaches is the distribution of contact normal vector $P(\mathbf{n})$.

The overall homogenization scheme further requires, in addition to the interparticle contact law, an averaging operation and a so-called "localization" relationship. Depending on the assumptions for the localization and averaging operations, several constitutive equations can be derived. The two classical results presented hereafter provide upper and lower bounds of the actual behavior. The contact law is assumed to be linear elastic and characterized by the normal and tangential contact stiffness k_N and k_T.

As mentioned is Section 3, the description of contact between two elliptical grains requires the knowledge of the three orientations θ, θ_a and θ_b instead of only θ for contact between two circular particles.

5.1. Kinematic scheme

The kinematic scheme corresponds to a uniform strain assumption within the RVE. The contact interpenetration increment Δu_i can be related to the applied strain increment $\Delta\varepsilon_{ij}$ by:

$$\Delta u_i = \Delta\varepsilon_{ij} l_j \tag{8}$$

The linear elastic interparticle contact law can be written as:

$$\Delta F_i = k_N \Delta u_N n_i + k_T \Delta u_T t_i = [k_N n_i n_j + k_T[\delta_{ij} - n_i n_j]]\,\Delta u_j = K_{ij}\,\Delta u_j \tag{9}$$

where Δu_N and Δu_T are the normal and tangential components of the contact interpenetration increment, n_i and t_i are the normal and tangential contact unit vectors and δ_{ij} is the Kronecker unit tensor.

The overall resulting stress increment is then determined by the averaging operation:

$$\Delta\sigma_{ij} = \frac{1}{V}\sum_{\text{contacts}} \Delta F_i l_j = \frac{N}{V}\int_{\theta=0}^{2\pi}\int_{\theta_a=-\pi/2}^{\pi/2}\int_{\theta_b=-\pi/2}^{\pi/2} \Delta F_i l_j P(\theta,\theta_a,\theta_b)\,\mathrm{d}\theta\,\mathrm{d}\theta_a\,\mathrm{d}\theta_b \tag{10}$$

where N is the total number of contacts within the volume V.

Once the distribution of the three statistical variables $P(\theta,\theta_a,\theta_b)$ is known, the branch vector can be easily derived for any θ, θ_a and θ_b and the localization operation applied. The integration corresponding to the averaging operation generally requires a numerical evaluation. As shown in Section 3, $P(\theta,\theta_a,\theta_b)$ depends on both the shape factor and the initial particle arrangement while the branch vector only depends on θ, θ_a, θ_b and the shape factor a^2.

5.2. Static scheme

The static scheme corresponds to a uniform stress assumption within the RVE. It requires the definition of the fabric tensor F_{ij} and its inverse A_{ij} where:

$$F_{ij} = \frac{1}{V} \sum_{\text{contacts}} l_i n_j = \frac{N}{V} \int\int\int l_i n_j P(\theta, \theta_a, \theta_b)\, d\theta\, d\theta_a\, d\theta_b \tag{11}$$

The contact force increment ΔF_i can then be related to the applied stress increment $\Delta\sigma_{ij}$ by (Chang and Liao, 1994):

$$\Delta F_i = \Delta\sigma_{ij} n_k A_{kj} \tag{12}$$

The linear elastic contact law is further used to determine the increment of contact interpenetration Δu_j to introduce in the averaging operation (Chang and Liao, 1994):

$$\Delta\varepsilon_{ij} = \frac{1}{V} \sum_{\text{contacts}} A_{ij} n_k \Delta u_j = \frac{N}{V} \int\int\int A_{ij} n_k \Delta u_j P(\theta, \theta_a, \theta_b)\, d\theta\, d\theta_a\, d\theta_b \tag{13}$$

The determination of the fabric tensor requires the knowledge of the distribution of the three statistical variables $P(\theta, \theta_a, \theta_b)$. Then a process similar to that presented in Section 5.1 leads to the numerical assessment of the global elastic characteristics of the granular media.

5.3. Comparison with numerical results

The numerical results have been compared with the homogenization approach (kinematic and static schemes) in the isotropic and anisotropic cases. For isotropic case (Case 1), Eqs. (10) and (13) rewrite:

$$\Delta\sigma_{ij} = \frac{N}{2\pi V} \int_{\theta=0}^{2\pi} \int_{\theta_a=-\pi/2}^{\pi/2} \int_{\theta_b=-\pi/2}^{\pi/2} \Delta F_i l_j P(\theta_a) P(\theta_b)\, d\theta\, d\theta_a\, d\theta_b \tag{14}$$

$$\Delta\varepsilon_{ij} = \frac{N}{2\pi V} \int\int\int A_{ij} n_k \Delta u_j P(\theta_a) P(\theta_b)\, d\theta\, d\theta_a\, d\theta_b \tag{15}$$

with $P(\theta_a)$ and $P(\theta_b)$ given by Eq. (2).

For anisotropic cases 2 and 3, Eqs. (10) and (13) rewrite:

$$\Delta\sigma_{ij} = \frac{N}{V} \int_{\theta=0}^{2\pi} \int_{\theta_a=-\pi/2}^{\pi/2} \int_{\theta_b=-\pi/2}^{\pi/2} \Delta F_i l_j P(\theta) P_{\text{aniso}}(\theta, \theta_a) P_{\text{aniso}}(\theta, \theta_b)\, d\theta\, d\theta_a\, d\theta_b \tag{16}$$

$$\Delta\varepsilon_{ij} = \frac{N}{2\pi V} \int\int\int A_{ij} n_k \Delta u_j P(\theta) P_{\text{aniso}}(\theta, \theta_a) P_{\text{aniso}}(\theta, \theta_b)\, d\theta\, d\theta_a\, d\theta_b \tag{17}$$

where $P_{\text{aniso}}(\theta, \theta_a)$ and $P_{\text{aniso}}(\theta, \theta_b)$ are given by Eq. (5) and $P(\theta)$ by Eq. (3).

The values of N and V are determined directly on the initial states of each sample.

The results provided by the kinematic scheme are close to the numerical ones. Furthermore it appears that the proposed expression for the probability of orientations θ_a and θ_b is necessary to capture the decrease of the elastic modulus for aspect ratios greater than 1.5. This trend can not be obtained if one considers isotropic distributions for θ, θ_a and θ_b (Fig. 13). The use of the static scheme leads to similar results even though it is shown that Young's modulus is proportional to the fabric tensor. Nevertheless, discrepancies are observed between numerical and theoretical results that can be explained by the inaccuracy of the distributions of θ_a and θ_b for a^2 greater than 1.0 (see for example Fig. 7a) but also by the homogenization approach itself (discrepancy observed for $a^2 = 1.0$).

In the anisotropic Cases 2 and 3, the elastic moduli in the vertical and horizontal directions have been estimated either by the kinematic or static approaches. Since the results are very similar, Fig. 14 only presents the results obtained for the latter. Both Eqs. (5) and (6) have been used together with the anisotropic distribution of the contact plane orientation (Eq. 3). It appears that, although the trends are

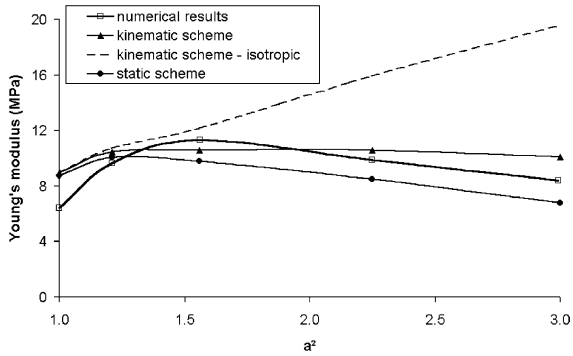

Fig. 13. Variation of Young's modulus with a^2, Case 1 (numerical and theoretical results).

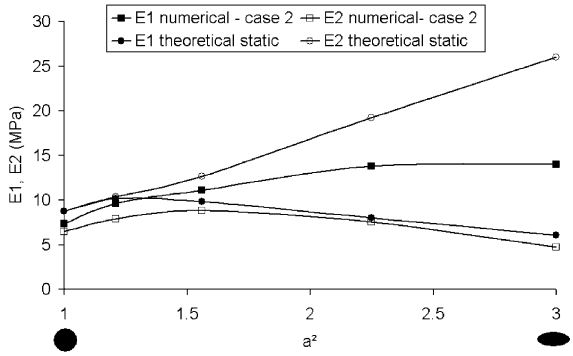

Fig. 14. Variation of elastic moduli E_1 and E_2 with a.

correctly captured, the approach fails to reproduce the exact values of E_1 and E_2. In this case, the discrepancies are mainly due to the inaccuracy of the distributions of θ_a and θ_b even for $a^2 = 1.0$.

6. Conclusion

The statistical homogenization approach proposed to determine the characteristics of granular media consisting in elliptical particles and its comparison with DEM results proves that an accurate description of the distribution of contact plane orientation and relative particle orientation to the contact plane is required.

In the isotropic case, the predicted results are in good agreement with the numerical ones even though the considered range of particles eccentricities is large. On the contrary for anisotropic assemblies, a more refined description of statistical variables and their correlation is necessary to capture the variation of the mechanical properties with the particles aspect ratio. A first improvement has been proposed.

This paper focused on the linear elasticity of the granular material. Further research will tackle the theoretical determination of the shear strength characteristics of assemblies of elliptical grains. Results of DEM simulation of biaxial compression tests are already available (with a large range of particle aspect ratios).

References

Aloufi, M., Santamarina, J.C., 1995. Low and high strain macrobehaviour of grains masses—the effect of particle eccentricity. Trans. Am. Soc. Agric. Eng. 38 (3), 877–887.

Cambou, B., Dubujet, P., Emeriault, F., Sidoroff, F., 1995. Homogenization for granular materials. Eur. J. Mech. A/Solids 14 (2), 255–276.

Chang, C.S., Liao, C.L., 1994. Estimates of elastic modulus for media of randomly packed granules. Appl. Mech. Rev. 47 (1, part 2), 197–206.

Claquin, C., 2003. Étude du Comportement de l'interface Milieu Granulaire et Inclusion par une Approche Multi-échelle. Ph.D. Thesis (in French). INSA de Lyon, France. p. 263.

Dong, J.-J., Pan, Y.-W., 1999. Micromechanics model for elastic stiffness of non-spherical granular assembly. Int. J. Num. Anal. Methods Geomech. 23, 1075–1100.

Emeriault, F., 1997. Anisotropic elasticity of granular assemblies with ellipsoidal elements. In: Mechanics of Deformation and Flow of Particulate Materials, June 29–July 2 1997. ASCE. Evanston, Illinois, New York. pp. 47–61.

Emeriault, F., Cambou, B., 1996. Micromechanical modelling of anisotropic non-linear elasticity of granular medium. Int. J. Solids Struct. 33 (18), 2591–2607.

Emeriault, F., Cambou, B., Mahboubi, A., 1996. Homogenization for granular materials: non-reversible behaviour. Mech. Cohes.-Frict. Mater. 1, 199–218.

Emeriault, F., Claquin, C., 2000. Micromechanical modelling of the anisotropic viscoelasticity of granular materials: statistical homogenization. Granul. Matter 2, 201–210.

Emeriault, F., Claquin, C., 2003. Statistical homogenisation for assemblies of elliptical grains: effect of the aspect ratio and particle orientation. In: Proceedings of QuaDPM'03 Workshop, Budapest, Hungary. p. 8.

Itasca Consulting Group, 1999. Particle flow code in 2 dimensions. Version 2.

Mahboubi, A., 1995. Contribution à l'étude Micromécanique du Comportement des Matériaux Granulaires par Homogénéisation et Approche numérique. Ph.D. Thesis (in French). Ecole Centrale de Lyon, France. p. 217.

Ng, T.-T., 1994. Numerical simulations of granular soil using elliptical particles. Comput. Geotech. 16, 153–169.

Ng, T.-T., 1999. Fabric study of granular materials after compaction. J. Eng. Mech. 125 (12), 1390–1394.

Ng, T.-T., 2001. Fabric evolution of ellipsoidal arrays with different particle shapes. J. Eng. Mech. 127 (10), 994–999.

Rothenburg, L., Bathurst, R.J., 1991. Numerical simulation of idealized granular assemblies with plane elliptical particles. Comput. Géotech. 11, 315–329.

Rothenburg, L., Bathurst, R.J., 1992. Micromechanical features of granular assemblies with planar elliptical particles. Gotechnique 42 (1), 79–95.

Ting, J.M., Khwaja, M., Meachum, L.R., Rowell, J.D., 1993. An ellipse-based discrete element model for granular materials. Int. J. Num. Anal. Methods Geomech. 17, 603–623.

Ting, J.M., Meachum, L.R., Rowell, J.D., 1995. Effect of particle shape on the strength and deformation mechanisms of ellipse-shaped granular assemblages. Eng. Comput. 12, 99–108.